Nanoscale

RSC Publishing

FEATURE ARTICLE

View Article Online
View Journal | View Issue

Advanced gecko-foot-mimetic dry adhesives based on carbon nanotubes

Cite this: *Nanoscale*, 2013, **5**, 475

Shihao Hu,[a] Zhenhai Xia[b] and Liming Dai*[a]

Geckos can run freely on vertical walls and even ceilings. Recent studies have discovered that gecko's extraordinary climbing ability comes from a remarkable design of nature with nanoscale beta-keratin elastic hairs on their feet and toes, which collectively generate sufficiently strong van der Waals force to hold the animal onto an opposing surface while at the same time disengaging at will. Vertically aligned carbon nanotube (VA-CNT) arrays, resembling gecko's adhesive foot hairs with additional superior mechanical, chemical and electrical properties, have been demonstrated to be a promising candidate for advanced fibrillar dry adhesives. The VA-CNT arrays with tailor-made hierarchical structures can be patterned and/or transferred onto various flexible substrates, including responsive polymers. This, together with recent advances in nanofabrication techniques, could offer 'smart' dry adhesives for various potential applications, even where traditional adhesives cannot be used. A detailed understanding of the underlying mechanisms governing the material properties and adhesion performances is critical to the design and fabrication of gecko inspired CNT dry adhesives of practical significance. In this feature article, we present an overview of recent progress in both fundamental and applied frontiers for the development of CNT-based adhesives by summarizing important studies in this exciting field, including our own work.

Received 4th October 2012
Accepted 6th November 2012

DOI: 10.1039/c2nr33027j

www.rsc.org/nanoscale

1 Introduction

Geckos can maneuver on almost any surface at any angle with ease, whether it is smooth or rough, wet or dry, vertical or even inverted.[1–3] Geckos' prominent climbing abilities stem from the hierarchical fibrillar structures of the beta-keratin foot hairs on their toe pads, which are known as setae[4–6] (Fig. 1a–c). Thousands to millions of high-aspect-ratio micro-sized setae form

[a]*Center of Advanced Science and Engineering for Carbon (Case4Carbon), Department of Macromolecular Science and Engineering, Case School of Engineering, Case Western Reserve University, 10900 Euclid Avenue, Cleveland, Ohio 44106, USA. E-mail: liming.dai@case.edu*

[b]*Department of Materials Science and Engineering, Department of Chemistry, University of North Texas, Denton, TX 76203, USA*

Shihao Hu received his PhD in Mechanical Engineering from The University of Akron in August 2012, where he used both simulation and experimental means to study natural and synthetic fibrillar adhesive systems, as well as advanced nanocomposites. He has a background in the interdisciplinary interfaces between materials science, applied mechanics and biomimicry. Hu is now a postdoctoral research associate in the Macromolecular Science and Engineering Department at Case Western Reserve University, and working to develop gecko-inspired self-cleaning adhesives by integrating carbon nanomaterials with polymers.

Zhenhai Xia received his PhD degrees in Materials Science and Engineering from Northwestern Polytechnic University of China in 1990. He is now an Associate Professor of materials science and engineering of the University of North Texas. His current research interests are focused on nanomechanics and nanomaterials, biomimetic materials, catalysts for clean energy and multiscale modeling and simulation.

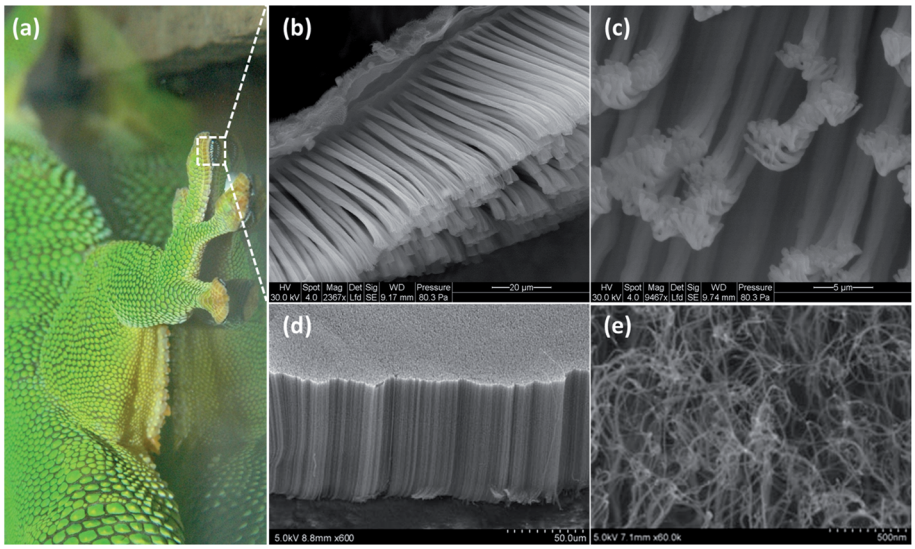

Fig. 1 (a) Picture of a day gecko foot attached on a glass substrate. SEM images of (b) a setal array and (c) a close-up showing spatulae at the tip; (d) vertically aligned carbon nanotube array with (e) entangled top layer. (a–c) Courtesy from Peter H. Niewiarowski at The University of Akron; credit: Edward Ramirez. (d and e) Adapted from ref. 28 with permission. Copyright (2008) The American Association for the Advancement of Science.

densely packed setal arrays (Fig. 1b) and each single seta further splits into hundreds of nano-sized spatulae at the tip (Fig. 1c). Intimate contacts of the individual fibrils to a broad range of surface topography are readily formalized when geckos place their feet onto the substrate,[7–9] which generates a formidable adhesion collectively *via* the ubiquitous nonselective van der Waals (vdW) interactions.[10–12] The maximum adhesive force of a single seta was measured to be as high as ~200 μN in shear and ~40 μN in normal against a smooth clean glass substrate.[10,11] Atomic force microscopy (AFM) has also revealed a normal pull-off force of ~10 nN for individual spatulae.[13] Thus, if all the setae, about half a million on one gecko foot, were to engage at a time, a single foot of gecko could generate ~100 N of adhesive force. Nevertheless, typically <~10 N of force is measured for a single foot at the whole animal scale.[1] Although vdW force has been proven to be the primary molecular origin for gecko's extraordinarily climbing ability, humidity does have a strong effect on the 'dry' adhesion of gecko setae.[14–16]

The discovery that the vdW interactions are responsible for the gecko foot adhesion has stimulated a great deal of interest in the scientific community for more than a decade now. Since the early demonstration of a dry adhesive tape consisting of electron beam defined polymeric nano-rods in 2003,[17] two major types of materials (namely, synthetic polymers and carbon nanotubes, CNTs) have been studied as alternative candidates for creating gecko-foot-mimetic dry adhesives.[18–21] Because the geometries/morphologies of polymeric fibrils are relatively easy to control by using various micro-/nano-fabrication techniques (*e.g.*, cast-molding and lithography), polymers became a popular choice, especially in the early development stage. This fabrication versatility (*i.e.*, the 'top-down' approach) allows for very sophisticated gecko-foot features, such as angled stalks, 3D tip shapes and hierarchy, to be incorporated into the polymeric versions.[22–26] However, practical applications of polymeric fibrillar dry adhesives are severely limited by their poor mechanical properties. Although some polymers (*e.g.*, poly(methyl methacrylate), PMMA and polyurethane acrylate, PUA) have a Young's modulus and/or tensile strength similar to that of the keratinous setae, the robustness of polymeric fibrils for cyclic use is still not comparable to their natural counterparts. The higher the elastic/yield strength the individual fibrils possess the better cyclic performance the adhesive patch will achieve.

CNTs, on the other hand, are suitable for creating strong and reversible fibrillar adhesives with a great durability due to their superior structural and mechanical properties (*i.e.*, 'smaller' and 'stronger' than gecko spatulae), even under severe environmental conditions (*e.g.*, extremely high and/or low temperatures).[27] Indeed, Qu *et al.*[28] have demonstrated that vertically aligned carbon nanotube (VA-CNT) arrays (Fig. 1d) with an

Liming Dai is the Kent Hale Smith Professor in the Department of Macromolecular Science and Engineering at Case Western Reserve University (CWRU). He is also director of the Center of Advanced Science and Engineering for Carbon (CASE4-Carbon). Before joining the CWRU, he was an associate professor of polymer engineering at the University of Akron and the Wright Brothers Institute Endowed Chair Professor of Nanomaterials at the University of Dayton. Dr Dai's expertise lies across the synthesis, chemical modification and device fabrication of conjugated polymers and carbon nanomaterials for energy-related and biomedical applications.

entangled top layer (Fig. 1e) could generate a macroscopic adhesive force 10 times that of a gecko's foot.[1] The potentials of CNT based fibrillar adhesives, however, are far from being fully exploited, although much progress has been achieved in recent years (see following sections). In general, compared to polymeric dry adhesives and even natural gecko foot hairs, the use of CNTs as the basic building blocks for advanced fibrillar adhesives provides multiple advantages, including, but not limited to: (i) great structural and mechanical strength for reversible and reusable purposes; (ii) high thermal conductivity and stability for high/low temperature applications as well as thermal management; (iii) excellent electrical and electrochemical properties for conductive adhesives and electrodes. In this feature article, recent progress in the development of CNT-based advanced fibrillar adhesives is reviewed, along with discussions on current challenges and future directions, aiming to provide not only some practical perspectives but also deep insights into this fast growing field of biomimicry.

2 VA-CNT arrays as gecko inspired fibrillar adhesives

Chemical vapor deposition (CVD) has been most widely used to grow VA-CNT arrays on quartz or silicon substrates. The aspect ratio, tube diameter and packing density of the resultant CNT arrays could be strictly tuned by adjusting precursors, catalysts as well as the vapor deposition conditions.[29–31] Various aspects of the mechanical properties of VA-CNTs, related to tribological and adhesive characteristics,[32] have been carefully evaluated while their thermal and electrical properties have also been investigated to a great extent.[29,33–36] In what follows, we highlight the important issues governing the adhesive performance of VA-CNT arrays: namely (i) compressive frictional responses (*i.e.*, tribology); (ii) adhesive forces (*i.e.*, interfacial adhesion and friction forces corresponding to the external normal and shear loadings, respectively); (iii) CNT transfer to increase substrate bonding; (iv) patterned CNTs and (v) hierarchical CNT structures for dry adhesions.

2.1 Mechanical responses of VA-CNT arrays under compression

Since a significant amount of preloading is often needed to initialize a large fraction of real contact for achieving strong adhesive forces using VA-CNT arrays, Ge *et al.*,[37] systematically studied the mechanical responses of the VA-CNTs (patch size: 500 μm × 500 μm and 3 mm × 3 mm area; 200–500 μm in height) by applying incremental compressive loadings along both the longitudinal and transverse directions of the CNT bundles (Fig. 2a and b; see insets, respectively). Nonlinear stress–strain curves were obtained with three distinctive sub-linear regions when longitudinally compressed (Fig. 2a). The effective/bulk Young's moduli transformed from an initially low value to a higher value and then returning to a lower level again (Fig. 2a). In contrast, the transverse compression resulted in an almost monotonic increase of the effective moduli (Fig. 2b).

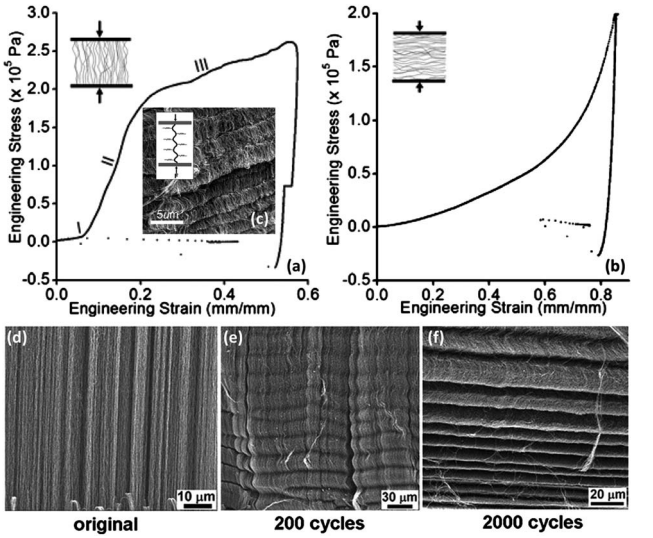

Fig. 2 Anisotropic compression moduli of multi-walled vertically aligned carbon nanotube arrays. Stress–strain curves obtained when compressed (a) parallel and (b) perpendicular to the aligned tube orientation of the VA-CNTs. SEM images of (c) the periodical buckling of a VA-CNT array; and a 1.2 mm thick CNT film (d) before, (e) after 200 cycles and (f) after 2000 cycles of compression, showing the evolution of periodic buckling with increasing loading cycles. (a–c) Adapted with permission from ref. 37. Copyright (2010) American Chemical Society. (d–f) Adapted with permission from ref. 38. Copyright (2005) The American Association for the Advancement of Science.

A cooperative deformation mechanism was proposed by considering a balance between 'long wave bucking' and 'short wave bending' that was determined by the constraint spacing between neighboring CNTs and individual nanotube bending stiffness, respectively. The predicted periodical bucking of the CNT bundles under compression agrees well with the experimental observations from high-resolution side-view SEM images (Fig. 2c). The bending recovered at lower stains (5–10%), but irreversible deformation happened especially for thinner tubes (*i.e.*, 8 nm *vs.* 40 nm) at higher strains. Transversely, the stress increased parabolically with strain and the strong adhesion between neighboring CNTs prevented the recovery of compressed bundles, suggesting that the CNT patch under severe shear loading underwent irreversible deformation. This could be one of the main factors limiting reusability. It was also evident that the CNT buckling could lead to a sidewall line contact at the interface to enlarge the real contact area, and as a result, both the normal and shear pulling forces increased linearly with increasing preloading. These findings are consistent with the work done by Qu *et al.*,[28] [*vide infra*], whether the sidewall contact was pre-existing or generated by compression.

In fact, CNTs are super strong, elastic and resilient materials even under very large compressions. As demonstrated by Cao *et al.*,[38] freestanding films of VA-CNTs exhibited super-compressible foam-like behavior. The VA-CNTs could be compressed to less than 15% of their original thickness (*i.e.*, ~860 μm) but still almost instantaneously bounced back to the original state (recovery rate > 2000 μm s^{-1}) upon stress removal. Full recovery was recorded for hundreds of cycles and gradually a maximum of 20% thickness reduction was built up beyond

10 000 cycles (Fig. 2d–f). The compressive strength of the 'foam-like' CNT materials was determined to be 12–15 MPa, roughly 10 times that of a polymeric open-cell foam structure from latex rubber or polyurethane can achieve. Besides, the stress loop (*i.e.*, hysteresis) indicates large energy absorption during a loading cycle attributable to the friction between CNTs and the disturbing air that possibly damps the dynamic motion. Another piece of important work concerning the compressive responses of VA-CNT arrays was carried out by Tong *et al.*[39] Almost invariant effective compressive moduli (~0.25 MPa) were captured for CNT lengths ranging from 15 to 500 μm using a home-built optically probed loading platform. The modulus lies well within the empirical Dahlquist criterion for tacky materials, which is also the feature found in gecko setal arrays.[40] These authors also proposed a continuum model to interpret the experimental observations considering different buckling modes and their mixture with bending. These spectacular mechanical properties of VA-CNTs make them extremely suitable for gecko inspired fibrillar adhesives. As we can see from discussions in subsequent sections, however, the substrate bonding strength and morphological tailorability still need to be further improved before the CNT based dry adhesives of practical significance could be used in demanding environments (*e.g.*, high/low temperature, humidity) with great reusability, and even surpass that of gecko feet.

2.2 Tribological behaviors of VA-CNT arrays

Strong friction forces for a 6 μm thick VA-CNT film were firstly reported by Kinoshita *et al.*[41] The frictional responses were found to be governed by the Amontons–Coulumb frictional law with a high frictional coefficient ($\mu = 1.7$) primarily due to the bending deformation of the nanotubes under longitudinal compression. The friction forces were independent of either the sliding speed (0.15–24 μm s^{-1}) or probe radii (gold tips with apex radii from 4.5 to 30 μm). However, no adhesion force was observed for this thin-film-like VA-CNT array. Subsequent study performed by Lu *et al.*[42] demonstrated that a much shorter VA-CNT array (~30 nm) extruded from anodic aluminum oxide (AAO) templates rendered very low friction forces. These two studies suggest that the length of CNT is crucial for regulating the friction forces under normal compressive loadings. Using a micro-tribometer, Dickrell *et al.*[43] studied the orientation dependence of the tribological behaviors for multiwalled carbon nanotubes (MWCNTs). In this study, vertically aligned MWCNTs with a thickness of 40–80 μm were prepared on quartz substrates by CVD, from which horizontally aligned MWCNTs with a thickness of 2–10 μm were prepared by mechanical scratching. A high friction coefficient ($\mu \cong 0.795$) was found for the MWCNTs aligned normal to the contact plane whereas the same MWCNTs lying flat showed a very low friction coefficient ($\mu \cong 0.090$). Therefore, friction could be tuned by controlling the nanotube orientation and morphology.

2.3 Nanoscale adhesion and friction between individual CNTs relevant to VA-CNT arrays

As advantages of adopting CNTs for creating fibrillar dry adhesives became clear, many groups studied the adhesion, friction, and general mechanical behaviors of individual CNTs against certain substrates, along with the nanotube–nanotube interactions. These studies help us to understand the complex responses of the VA-CNT arrays as a whole, and shed light on the underlying mechanism that governs their macroscopic adhesive performances.

For instance, Maeno *et al.*[44] employed a transmission electron microscope (TEM) system equipped with two manipulation stages to examine the adhesion strength (*i.e.*, pull-off force) at the nanoscale contact (in a flat–flat configuration) between a single CNT tip and two different solid surfaces of Au and SiO_2, respectively. In both cases, it was found that the normal adhesion has a linear relationship with the cross-sectional area of the CNT. The highest adhesion, 6.84 nN, was recorded for a CNT tip of ~30 nm^2 area interacting with the Au substrate. The Hamaker constant for the CNTs was estimated to be around $4.0–8.9 \times 10^{-20}$ J.

By attaching individual CNTs vertically onto the apex of AFM cantilevers (Fig. 3a), Bhushan *et al.*[32] studied the adhesive behaviors of single MWCNT against various target surfaces, including single-crystal silicon, single-crystal aluminum, mica sheet, and gold film. During a typical measurement, the CNT probe was pressed perpendicularly onto the target surface until it bended, buckled, and completely deflected and deformed into a laterally lying configuration (*i.e.*, from a tip contact to a line contact), and then pulled off backwards in the vertical direction until complete separation from the target surface. By so doing, the critical buckling force was measured to be about 20 nN for the MWCNT with ~20 nm diameter and 2 μm protrusion. The MWCNT adhesion force was found to lie in the range of 100–190 nN for the substrates studied. Both a 'buckle-in' and a 'jump-off' event of the CNT tip were clearly captured during the compressing and retracting stages, respectively (Fig. 3b). Frictional behaviors were also singled out from the whole scenarios of compression and retraction. Compared to Si tips, CNT tips were demonstrated to have a lower wear on the Au film, suggesting a promise for AFM imaging and manipulations.

In a separate study, Bhushan *et al.*[45] have further investigated the adhesion and friction at crossed nanotube junctions in ambient temperature using AFM in tapping mode. They found that the coefficient of friction between nanotubes was about 0.006 ± 0.003, and that the frictional behavior between nanotubes could be altered by ambient water, which accounts for the force discrepancy from the vacuum condition. Utilizing the interactions between fiber to fiber contacts, Ko *et al.*[46] created a flexible self-selective connector from vertically aligned carbon nanofiber (VA-CNF) arrays to show excellent anisotropic adhesive behaviors with a strong shear but a weak normal adhesion strength.

Along with the adhesion measurements, peeling tests are also of paramount importance, especially for CNT arrays with pre-existing entangled segments on top.[28] In this context, Strus *et al.*[47] and Ishikawa *et al.*[48,49] have attached individual CNTs parallel to an AFM cantilever (*e.g.*, Fig. 3c) and tested single CNT peeling. Both groups captured the coexistence of different tube configurations: from a straight one-dimensional CNT nanostructure lying on the substrate transformed into an s-shape, arc-shape, and finally a freestanding state (captured in the simulation

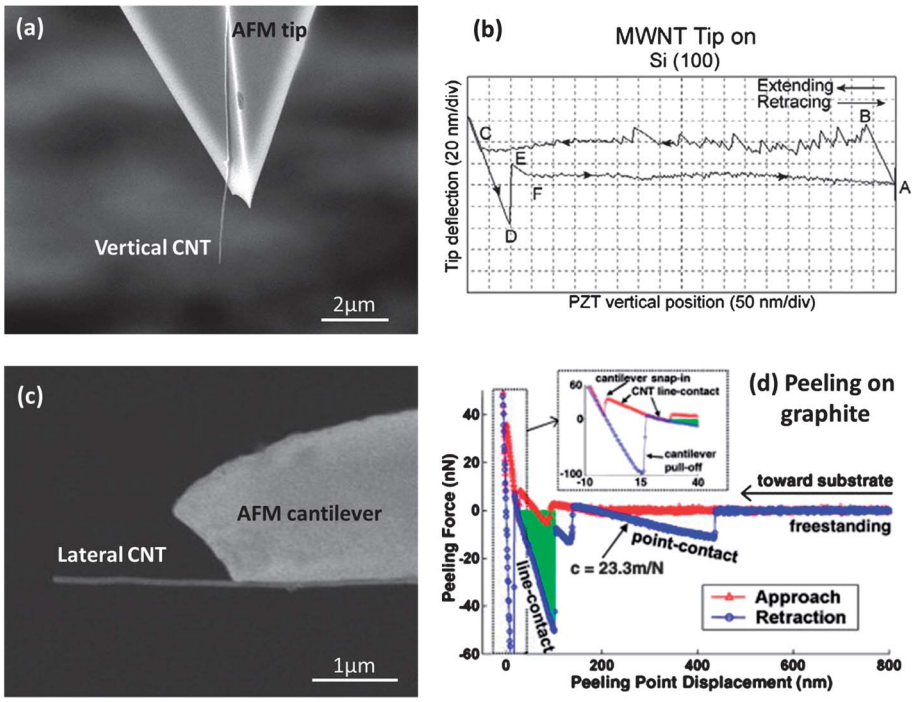

Fig. 3 (a) SEM image of a MWCNT attached on the apex of an AFM tip in a vertical configuration. (b) Force calibration plots using the vertical MWCNT tip against a Si substrate. (c) SEM image of a MWCNT attached on the underside of an AFM cantilever in a horizontal configuration. (d) Peeling force curves for the lateral CNT probe as a function of peeling point displacement on graphite. (a and b) Reproduced with permission from ref. 32. Copyright (2008) IOP Publishing. (c and d) Reproduced with permission from ref. 50. Copyright (2009) Elsevier.

results discussed in Section 3 as well). The force displacement curves recorded during the retraction processes showed distinctive stick–slip phenomena for both the line and point contacts (Fig. 3d). In addition, Strus *et al.*[50] found that CNTs possessed a higher interfacial energy with epoxy (1.7 pJ m^{-1}) than graphite (1.1 pJ m^{-1}), whilst CNT-polyimides (0.6 pJ m^{-1}) showed the lowest among the three. It was noticed that the lateral forces (*i.e.*, friction) were not captured simultaneously in these nanofiber/nanotube peeling tests because of the 'translational limitations' for most AFMs. However a simulation approach could feasibly resolve these issues and enable one to investigate the force coupling between normal and shear directions at nanoscale under various loading conditions (*cf.* Section 3).

2.4 Nanoscale adhesive forces of VA-CNT arrays

For nanoscale adhesion measurements, Yurdumakan *et al.*[51] prepared VA-MWCNT arrays with a high aspect ratio (10–20 nm in diameter and ~50 μm in height). Having been transferred onto a PMMA substrate *via* an embedding and a subsequent etching process, the nano-level adhesive forces of the MWCNT array were measured against an AFM tip to be ~200 times higher than that of gecko foot hairs. However, the penetration of the AFM probe (rectangular silicon; typical radius curvature < 10 nm) into the arrays is responsible for this astonishingly high adhesive strength, where the side contacts and the entanglement of the CNTs with the probe tip could significantly increase the pull-off force. Thus, it is expected that this level of high adhesion may not be observed for a macroscopic contact when other factors, including tube rigidity, aspect ratio, spacing, and uniformity, come into consideration. Velocity independent behavior was recorded by changing the scan rate from 0.50 up to 14 Hz.

2.5 Macroscopic adhesive forces of VA-CNT arrays

Zhao *et al.*[52] characterized the macroscopic adhesive properties of VA-MWCNT arrays with a thickness of 5–10 μm (Fig. 4a–c). By pressing (*i.e.*, preload in normal; 2 kg weight) and subsequent pulling of the VA-MWCNT arrays in the normal or shear direction, these authors found the maximum adhesion strength of ~11.7 N cm^{-2} for an apparent contact area of 4 mm^2 and frictional strength of ~7.8 N cm^{-2} for an 8 mm^2 contact. These values are comparable to the gecko foot adhesion, showing the promise of using CNTs as robust structural elements to achieve high macroscopic dry adhesive forces. However, repeated measurements showed a poor CNT–substrate bonding, which limited the lifecycle to only a couple of times. Later, a macroscopic normal pull-off force of about 4 N cm^{-2} was reported by Wirth *et al.*,[53] for a 1 cm^2 area of ~100 μm thick VA-MWCNT patch. In this case, a relatively large preload was applied (100 N pressing for 30 seconds), leading to a detrimental damage of the CNT arrays. It was found that almost the entire VA-MWCNT array was pulled off from the Si substrate and matted onto the glass/plastic target surface after only one measurement.

Recently, Qu and Dai[29] successfully produced high quality vertically aligned single-walled carbon nanotubes (VA-SWCNTs; Fig. 4d–f) by a combined method of plasma-enhanced chemical vapor deposition (PECVD) and fast heating. SEM and Raman spectroscopic measurements revealed that constituent CNTs in the resultant VA-SWCNT arrays were semiconducting and

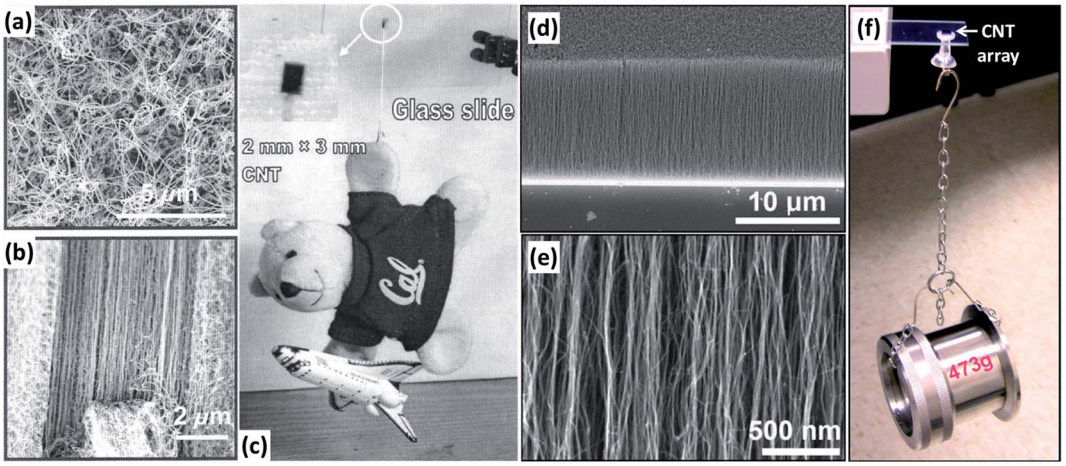

Fig. 4 SEM images of (a) top view and (b) side view of a VA-MWCNT array; and (c) a demonstration of its strength (2 × 3 mm^2 patch) using a toy bear with a space shuttle model in its right hand (total weight: 40 g). SEM images of (d) a cross-section view of a VA-SWCNT array and (e) the same as (d) under a higher magnification; and (f) a photo showing a stainless steel adapter of 473 g hanging on a VA-SWNT dry adhesive film (4 × 4 mm^2) supported by a SiO_2/Si wafer. (a–c) Reproduced with permission from ref. 52. Copyright (2006) American Institute of Physics. (d–f) Reproduced with permission from ref. 29. Copyright (2007) John Wiley and Sons.

uniformly distributed with almost no amorphous carbon. The smaller nanotube diameter, higher packing density, and more perfect electron rich π–π conjugated carbon structure are the three intrinsic characteristics associated with these VA-SWCNT arrays, which make them suitable for mimicking gecko foot adhesion. Indeed, the VA-SWCNT arrays were demonstrated to exhibit a much higher macroscopic adhesive force (29 N cm^{-2} for a 16 mm^2 patch; with 2 kg weight of preloading) than that previously reported for VA-MWCNT arrays and even the natural gecko feet (10 N cm^{-2}). Force-induced bending and buckling of the nanotube arrays into zigzag shapes significantly lowered the adhesion and friction strength after only couples of loading cycles. However, these VA-SWCNT dry adhesives showed an excellent thermal resistance due to the unique thermal and electric properties possessed by these SWCNTs.

In a subsequent study, Maeno and Nakayama[30] investigated the effects of CNT wall numbers on friction forces. Triple walled CNTs were demonstrated to have the appropriate flexibility for a conformal contact with rough surfaces while at the same time a good mechanical strength to resist buckling. It was also found that the VA-MWCNT array with a broad distribution of sidewall numbers adhered more effectively and showed a shear strength of 44.5 N cm^{-2} (a 1 cm^2 patch; 47 N of preloading *via* cylindrical roller) higher than that of SWCNTs. On this basis, these authors concluded that 'uniformity' may not be preferable for achieving large and robust contacts. Although tempting, this argument is very much debatable, since uniformity or similarity exist in most gecko adhesive systems. The structural hierarchy of individual fibrils (from setae to spatulae) renders an increased compliancy from stems to tip ends, which may be solely responsible for a greater conformability to compromise surface irregularities.

2.6 Transferring VA-CNT arrays onto flexible substrates

In order to improve the bonding of VA-CNTs to the underlying substrate, Yurdumakan *et al.*[51] have transferred the as-grown VA-MWCNTs from the Si substrate used for the nanotube growth onto a PMMA film. Later, Aksak *et al.*[54] used polyurethane elastomer, a polymeric material that is more flexible but with a higher tear resistance than PMMA, as the finishing substrate. After transfer, the tube length (exposed part: ~5 μm) became much more uniform as the exposed part was created by peeling the polymer-embedded CNTs away from the Si substrate and then selectively etching the polymer from the newly generated surface. Rigorous force measurements were implemented to study the friction and adhesion responses simultaneously for each approach–sliding–retraction cycle with a preprogrammed loading scheme. A hemispherical glass probe of 6 mm diameter was employed to alleviate the edge effects and deviations due to misalignment. The translational motion of the probe was fixed with a constant velocity of 5 μm s^{-1}. It was found that the effective friction coefficient (EFC) of the polymer-supported VA-MWCNTs remained constant (~0.9) when increasing the preloading to 50 mN. In contrast, controlled CNT samples on the Si substrate showed an EFC of 0.4 and 2.2 for 3 and 25 μm thick fiber arrays, respectively. Although the effect of changing substrate on the EFC is not conclusive, the cyclical performance was significantly promoted even under a very high compressive loading. On the other hand, the adhesion force was found to be trivial. Nevertheless, this type of 'adhesives' could find themselves useful in the situations where high friction but low adhesion is required, for instance, super grip tires and shoes.

2.7 Scaling up the patch sizes of VA-CNT arrays *via* predefined patterns

Ge *et al.*[55] utilized conventional photolithography to pre-define different patterns (width of squares: from 50 to 500 μm; Fig. 5a–d) of the catalyst on a silicon substrate and then selectively grew VA-MWCNTs (200–500 nm long, ~8 nm in diameter) on the areas covered by the catalyst. After transferring the resultant

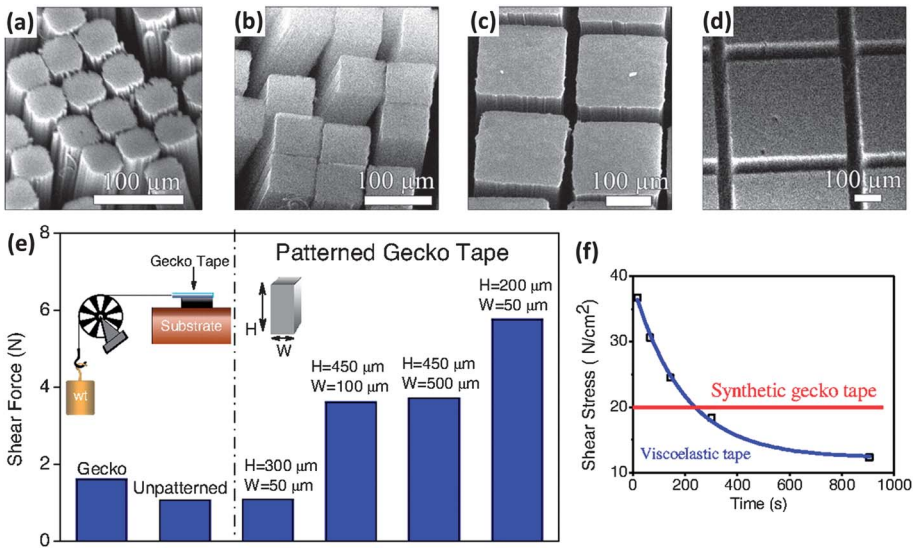

Fig. 5 SEM images of micro-fabricated VA-MWCNT patterns with width (a) 50 μm, (b) 100 μm, (c) 250 μm and (d) 500 μm. (e) The shear force supported by live gecko, unpatterned and patterned gecko tapes (0.16 cm^2 area) on mica substrates. Inset shows the geometry used in the shear measurements. (f) Different weights (*y* axis) were suspended on a viscoelastic tape using shear geometry, and the maximum time it can support that particular weight is plotted on the *x* axis. As a comparison, the 'gecko tapes' (0.16 cm^2 area with 500 μm wide patterns) supporting 20 N cm^{-2} shear force maintained the attachment over a period of 8–12 h, without any cohesive breakage. Reproduced from ref. 55 with permission. Copyright (2007) The National Academy of Sciences of the USA.

carbon nanotube patterns onto a flexible tape (3M Scotch tape), a shearing force of 36 N cm^{-2} was obtained for a 0.16 cm^2 patch under a preloading of 25–50 N cm^{-2} (Fig. 5e). Similar to the gecko setal arrays previously reported by Autumn *et al.*,[11] the shear forces for the VA-MWCNTs against hydrophobic and hydrophilic surfaces were about the same. In contrast, unlike viscoelastic tapes, the gecko-foot-mimetic CNT tapes showed time independent viscoelasticity and the shear force was maintained for 8–12 hours (Fig. 5f). Careful SEM examination after shear measurements revealed the rupture of CNTs and their residues at the interface, which is believed to be the evidence for a cohesive failure mechanism. It was found that the crack propagation could be effectively hindered by patterning the CNTs at microscale, leading to a significantly enhanced toughness under shear loadings. Peeling tests were carried out on different substrates to verify the easy releasing mechanism observed in gecko setal arrays.[2,9] In this light, a flexible backing support seems to not only render an enhanced substrate bonding with additional conformability for initializing an intimate contact but also to enable a feasible pealing-release mechanism for repeatable uses.

2.8 Hierarchical VA-CNT arrays with entangled top layers

Recent theoretical studies have indicated that maximized adhesion could be achieved by combining size-reduction and shape-optimization with hierarchical fibrillar structures.[7,8,56,57] Qu *et al.*[28] created hierarchical VA-CNT arrays with entangled nanotube segments on top of vertically aligned CNT trunks (Fig. 6a–c) through a low-pressure CVD process. Analogous to gecko setal arrays, this two-level VA-CNT structure features a straightly aligned body mimicking setal stalks, and curly entangled end segments on top mimicking spatulae. Under shear loading, the entangled segments contacted with the target surface through nanotube sidewalls and generated high macroscopic forces up to ~100 N cm^{-2} for a 0.16 cm^2 patch (Fig. 6d; 10 times that a gecko foot can afford). During the normal pulling process, however, each of the entangled segments was peeled off from the target surface through a 'point-by-point' failure mechanism, resulting in a significant reduction in the normal adhesion force (~10 N cm^{-2}; Fig. 6d). This directional dependency ensures a strong binding-on along the shear direction and an easy lifting-off in the normal direction (Fig. 6e), which is promising for mimicking live gecko walking.

It is of great importance to understand the structural changes at and near the top layer of the hierarchical VA-CNT array since the intermolecular forces between the nanotube array and the target surface (*e.g.*, glass slide) play a critical role in regulating its adhesive performance. As shown in Fig. 6d, the shear adhesion force increased with the increasing length of the nanotube trunks (or CNT film thickness) due to the increased contact area associated with the shear-induced alignment of the nonaligned nanotube top segments (the length of the top entangled segments increases with the increased vertical length or thickness of the films Fig. 6i–k) and improved conformability. In contrast, the normal adhesion force was almost insensitive to the nanotube trunk length (Fig. 6d) as the result of a distinctive detaching mechanism. As can be seen in Fig. 6f–h, the top non-aligned nanotube segments adapted randomly distributed 'line-lying' configurations on the glass substrate after initiating contact upon preloading. Under shear pulling, the external loading caused the nonaligned nanotube segments to orient and align uniformly along the shear direction against the glass substrate (Fig. 6i–k). Moreover, the vertically aligned nanotube trunks (Fig. 6l–n) tilted towards the shearing

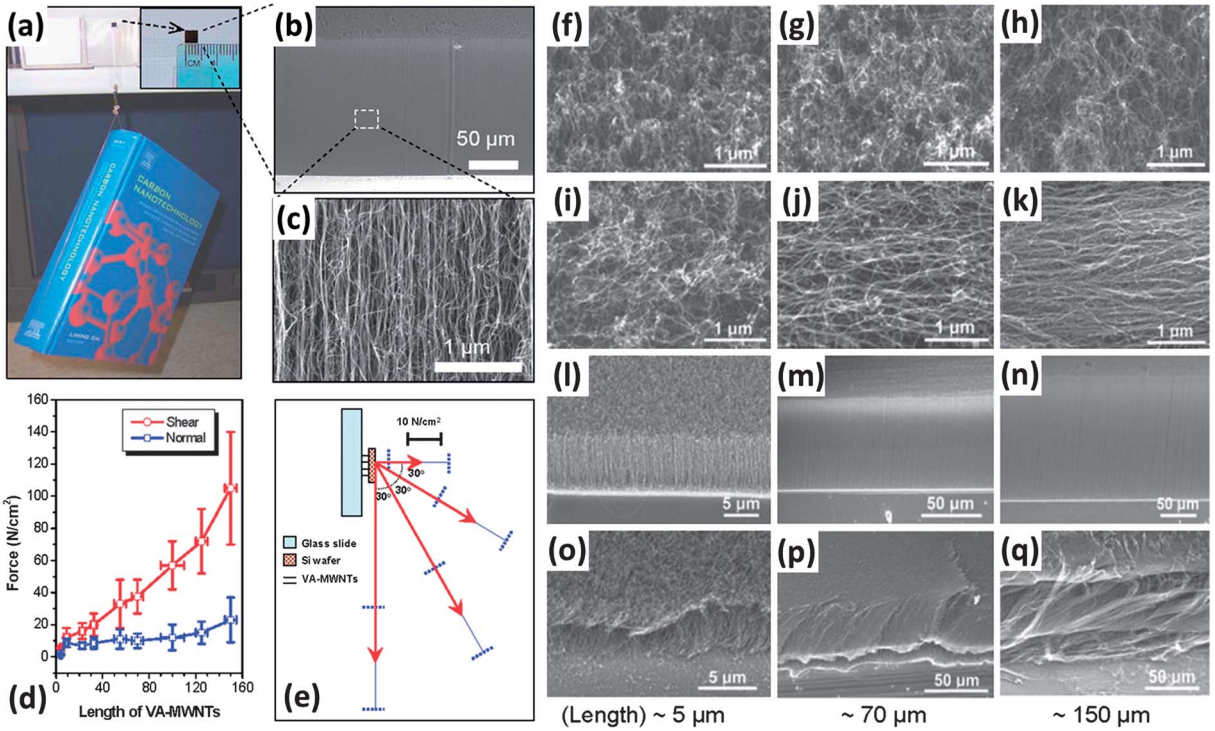

Fig. 6 (a) A book of 1480 g weight suspended from a glass surface *via* silicon wafer supported VA-MWCNTs. The top right squared area shows the VA-MWCNT array film, 4 × 4 mm^2. (b and c) SEM images under different magnifications. (d) Nanotube length-dependent adhesion force on glass with a preloading of 2 kg weight. (e) Adhesion strength with a length of 100 ± 10 μm at different pull-away directions. (f–q) SEM images for the morphological change of VA-MWCNT arrays during adhesion measurements. (f–k) Top and (l–q) side views with the lengths of (f, i, l and o) ~5 μm, (j, g, m and p) ~70 μm and (h, k, n and q) ~150 μm, (f–h and l–n) before and (i–k and o–q) after adhesion measurements. Error bars represent the deviations of the forces measured for more than 20 samples of a same class. Reproduced with permission from ref. 28. Copyright (2008) The American Association for the Advancement of Science.

direction (Fig. 6o–q), leading to a predominant aligned sidewall line contact with the glass surface which ensures a strong shear adhesion force. During normal pulling, however, the top nonaligned nanotube segments contacting with the glass substrate were peeled away from the substrate through a "point-by-point" detaching process, requiring a much lower external force. These failure modes have also been demonstrated by computer simulations (see Section 3 for details). The aforementioned sticking and detaching processes have also been demonstrated to occur on various other substrates with different flexibilities and surface characteristics, including glass plates, PTFE films, rough sandpapers, and PET sheets.[28] These findings pave the way to construct aligned CNT dry adhesives with a strong shear adhesion for firm attachment and relatively weak normal adhesion for easy removal, opening up many technological possibilities especially for locomotion applications at extreme conditions, for instance for outer space explorations and reversible adhesions at high temperatures.

2.9 Self-cleaning properties in VA-CNT arrays

Since most of the experimental force measurements on synthetic dry adhesives, including VA-CNT arrays, were carried out on smooth and clean surfaces, self-cleaning properties seem to be less important compared to the features such as adhesive strength, reversibility and reusability. However, self-cleaning is critical for repetitive attachment/detachment and locomotion purposes in the natural and usually 'contaminated' environment. A recent experiment has shown that even under extreme exposure to clogging particles, gecko setal arrays could recover enough adhesive function, after only four 'simulated steps'.[58] The understanding of the self-cleaning mechanism, however, is still preliminary,[21] and remains as a missing puzzle for explaining how geckos manage to keep their sticky feet clean while walking about around every day contaminants. As more and more gecko features are being incorporated into artificial mimicking systems, increasing attention has been focused on the self-cleaning properties in both gecko feet[59] and gecko-foot-mimetic systems.[60,61] Some recent studies along this line are described below.

Sethi *et al.*[61] investigated the self-cleaning properties of the patterned VA-MWCNT arrays.[55] Their CNT structured surfaces showed super-hydrophobicity (155 ± 3° static contact angle) resistant to multiple water exposures. After contaminating with silica particles ranging from 1 to 100 μm in size, the VA-CNT adhesives regained 60% or 90% frictional strength when rinsed with water or subjected to mechanical vibration, respectively. No significant macroscopic damage to the carbon nanotube pillars was observed after rinsing with water, but rather a limited amount of small microcracks was observed within the pillars after drying. Wirth *et al.*,[53] on the other hand, obtained contradictory results from static contact angle measurements.

These authors found that wetting behaviors of the VA-MWCNTs were very unstable. A change from the Cassie to Wenzel state[62,63] took place during water exposure, and the constituent aligned nanotubes matted and collapsed. These inconsistencies cannot be simply explained by whether or not the CNT is patterned but rather considering more morphological variations and the qualities of the CNTs. Moreover, the possible 'wet-cleaning ability' of VA-CNT adhesives is not the same as the self-cleaning property found in geckos, but rather a lotus effect.[64] As demonstrated by Hansen and Autumn,[58] geckos utilize a 'contact' self-cleaning mechanism, coupled with a low surface free energy feature of the toe pad structure, to keep their toes clean. The energy disequilibrium between the gecko toe pad/dirt particle interface and the dirt particle/target surface interface leads to the deposition of dirt particles on the surface, and hence gecko feet are self-cleaned by walking around. More recently, Hu *et al.*[59] proposed a unique dynamic self-cleaning mechanism that accounts for a much greater self-cleaning rate experienced at the whole animal scale, by considering the physiological behaviors of geckos toe peeling motion before taking each step. This phenomenon implies the importance of transferring VA-CNTs onto flexible and/or external-stimuli responsive backings. In this way, strong attachment, easy release and dynamic self-cleaning abilities could all be integrated into a single adhesive prototype. Last but not least, a recent publication indicates that geckos actually leave residues or foot prints, consisting of phospholipids, as they walk,[65] which provides another piece of evidence for explaining not only self-cleaning but also wear prevention, and even wet/underwater performance of the gecko setal arrays.[15,16] Therefore, functionalizing VA-CNT arrays with special coatings and/or incorporating them with stimuli-responsive materials and backings (*e.g.*, shape-memory polymers) could lead to multifunctional gecko inspired adhesives matching that of natural geckos and even beyond.

3 Multiscale modeling and simulation of hierarchical VA-CNT arrays

Along with advances in the experimental studies on the polymer and CNT-based gecko inspired dry adhesives discussed above, many groups have performed various theoretical analyses to elucidate the mechanics and mechanisms governing the performance of fibrillar dry adhesives.[12,66–73] However, most of the theoretical models are based on analytical derivations with a 'continuum' assumption. Great challenges emerge when the structure shrinks down to the nano-regime, where an emphasis on the nanoscale phenomena becomes more important and the 'continuum picture' breaks down.

In principle, all material properties are describable by quantum mechanics. However, the direct use of this exquisite theory is sometimes impractical, especially for systems with large numbers of atoms and/or molecules. Hence, special treatments across multiple scales are often essential. In this regard, Hu *et al.*[74,75] have developed a multiscale modeling and simulation approach to investigate the mechanical characteristics and processes for the prominent CNT dry adhesive with hierarchical fibrillar structures described in Section 2.8 (Qu *et al.*[28]). Specifically, a series of mechanical analyses at multiple time and length scales were constructed *via* molecular dynamics simulations and finite element methods, along with analytical derivations. Relations between the structures and adhesive properties were systematically established by linking the molecular configurations to the mesoscale geometries and the macroscale functions and performances.

As illustrated in Fig. 7, this multiscale computational framework spans three levels of structural hierarchy, ranging from atomistic molecular dynamics (*i.e.*, individual CNT peeling), through coarse grained molecular dynamics (*i.e.*, a fraction of the VA-CVT array being pulled normal and parallel with respect to the substrate), to finite elemental analysis (*i.e.*, device-level CNT patches under normal pulling and lateral shearing). Implementing atomistic molecular dynamic simulations to build the nanoscale peeling systems atom by atom and explicitly calculate the interaction force distributions at the interface along with the reaction forces at the pulling end for different boundary conditions, the missing picture in between the discrete and continuum levels could be completed.

In the nanoscale simulations, an atomistic level resolution was retained where the equations of motions between discreet atoms were calculated based on non-reactive force fields. By eliminating the electronic level resolution, one could study the effect of van der Waals interactions on the adhesive behaviors between the CNTs and the substrate with appropriate fundamental details but less computational expenses. Classical approximations were further carried out in the coarse-grained models to include complex tube–tube interactions as the systems were up-scaled into a higher level. At the ultimate functional level, phenomenological-based continuum methods were implemented to offer a feasible way of directly comparing and validating the simulation results with those from experimental measurements. Transitions and propagations between the models at different levels have also been addressed to give an insight into the potentials and limitations of this approach. As can be seen, the multiscale modeling and simulation

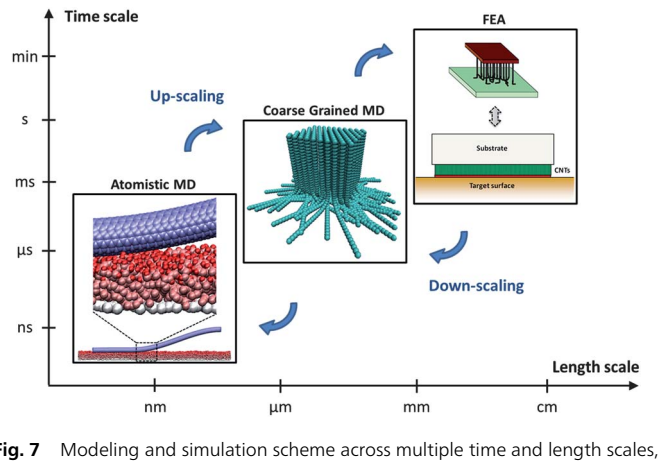

Fig. 7 Modeling and simulation scheme across multiple time and length scales, from fully atomistic to coarse grained molecular dynamics (MD) and to finite element analysis (FEA).

strategies shown in Fig. 7 form a closed loop *via* the up-scaling and down-scaling pathways.

Critical issues that were elucidated include (i) effects of the entangled CNT segments on the adhesion and friction behaviors at the nano-contact interface: the adhesion force is strongly enhanced by interfacial friction because of pre-existing asperities on the substrate, even with very tiny surface irregularities at the molecular or nanoscale; (ii) mechanics of local deformations in the lateral CNT peeling: significant local deformations and buckling of the carbon nanotubes were evident under the constrained peeling conditions, which is attributed to a mechanical interlocking mechanism at surface asperities. This effect results in drastically increased adhesive forces, whereas at the same time, could cause structural failure under cyclic loading and thus limit the serving life of CNT-based adhesives; (iii) force anisotropy and its transitions from the nano- to micro- and to macro-levels: with a second-level hierarchy, laterally distributed CNT segments on top of the vertically aligned CNT arrays, the adhesion force could be enhanced by a factor of 5 and 10 under macro-level pulling and nanoscale peeling, respectively. It also indicates that further improvement on force anisotropy could be achieved by controlling the morphology of the randomly oriented lateral segments to make them more informally distributed as that of gecko setae; and (iv) adhesion and friction force coupling that ensure an enhanced adhesion when shear engaged while relatively feasible to disengage at normal detachment: the critical peeling angle derived at the nano- and macro-scale simulations has been demonstrated to be intrinsically related to the adhesion enhancement factor, which is mostly dependent on the fiber/tube geometry and surface roughness, and relatively insensitive to the material types and mechanical properties. With the combinations of numerical simulations, analytical derivations, and experimental tests, further developments in the multiscale modeling and simulation approach should provide not only a detailed understanding of the underlying mechanisms governing the adhesive performance but also effective means to resolve the critical engineering issues in making gecko-foot-mimetic dry adhesives.

4 Summary and outlook

In summary, we have reviewed recent progress in the development of CNT-based advanced fibrillar adhesives. As can be seen, VA-CNT arrays exhibit many exquisite structural advantages as the basic building blocks for creating gecko-inspired fibrillar adhesives. Various high-quality VA-MWCNT and VA-SWCNT arrays with controllable tube structures and morphologies with longitudinal hierarchy (*e.g.*, CNT arrays with straight trunks and curled segments on top) have been successfully synthesized. Microfabrication methods have also been developed for patterning the aligned carbon nanotubes with a sub-micrometer resolution, and for transferring such nanotube arrays (*e.g.*, patterned/non-patterned) to various other substrates of particular interest (*e.g.*, polymer film as a flexible backing for VA-CNT dry adhesives). Judicious use of these VA-CNTs as building blocks for creating gecko inspired dry adhesives has led to the highest adhesive strength to date, $\sim$100 N cm^{-2}, which is $\sim$10 times that of a gecko foot.

Despite the fact that CNT-based gecko-foot-mimetic dry adhesives have been developed to show stronger adhesion than natural gecko feet and even with strong-binding along the shear direction and easy-lifting in the normal direction for simulating live gecko walking, the multifunctionalities of the natural gecko feet (*e.g.*, long lifecycle, wear prevention, and self-cleaning) have been scarcely studied and/or mimicked, though they are vital to 'smart' adhesives for many real-life applications. Surface-functionalization of the aligned carbon nanotubes to tailor their surface properties and/or compositing with stimuli-responsive materials (*e.g.*, functional polymers) could make CNT-based gecko-foot-mimetic adhesives multifunctional like natural gecko feet. However, many great challenges still lie ahead, including the poor scalability of existing synthetic methods for massive production of VA-CNTs, the required strong preloading force that often causes irreversible CNT buckling after repeated use, and short lifecycle. Recent and future findings from the biophysical and biochemical studies of gecko setal arrays (*e.g.*, the dynamic self-cleaning mechanism and the gecko footprint consisting of phospholipids), coupled with multiscale modeling and simulation approaches, should shed light on promising ways to develop gecko inspired CNT-based dry adhesives with further improved properties and new functionalities. To this end, the unique thermal and electrical features of CNTs could be exploited as additional assets in developing CNT-based adhesives outperforming the natural gecko feet, for example, with electrically switchable and high temperature tolerant properties. Continued research and development in this exciting field should be of great value, though challenging.

Acknowledgements

The authors are grateful for the financial support from NSF (NIRT0609077 and CMMI1047655), and would also like to thank colleagues and collaborators for their work cited in this article.

References

1 D. J. Irschick, C. C. Austin, K. Petren, R. N. Fisher, J. B. Losos and O. Ellers, *Biol. J. Linn. Soc.*, 1996, **59**, 21–35.
2 A. P. Russell, *Integr. Comp. Biol.*, 2002, **42**, 1154–1163.
3 K. Autumn and N. Gravish, *Philos. Trans. R. Soc., A*, 2008, **366**, 1575–1590.
4 P. F. A. Maderson, *Nature*, 1964, **203**, 780–781.
5 E. E. Williams and J. A. Peterson, *Science*, 1982, **215**, 1509–1511.
6 N. W. Rizzo, K. H. Gardner, D. J. Walls, N. M. Keiper-Hrynko, T. S. Ganzke and D. L. Hallahan, *J. R. Soc., Interface*, 2006, **3**, 441–451.
7 B. N. J. Perrson, *MRS Bull.*, 2007, **32**, 486–490.
8 H. Yao and H. Gao, *J. Mech. Phys. Solids*, 2006, **54**, 1120–1146.
9 K. Autumn, A. Dittmore, D. Santos, M. Spenko and M. Cutkosky, *J. Exp. Biol.*, 2006, **209**, 3569–3579.

10 K. Autumn, Y. A. Liang, S. T. Hsieh, W. Zesch, W. P. Chan, T. W. Kenny, R. Fearing and R. J. Full, *Nature*, 2000, **405**, 681–685.
11 K. Autumn, M. Sitti, Y. C. A. Liang, A. M. Peattie, W. R. Hansen, S. Sponberg, T. W. Kenny, R. Fearing, J. N. Israelachvili and R. J. Full, *Proc. Natl. Acad. Sci. U. S. A.*, 2002, **99**, 12252–12256.
12 Y. Tian, N. Pesika, H. Zeng, K. Rosenberg, B. Zhao, P. McGuiggan, K. Autumn and J. Israelachvili, *Proc. Natl. Acad. Sci. U. S. A.*, 2006, **103**, 19320–19325.
13 G. Huber, S. N. Gorb, R. Spolenak and E. Arzt, *Biol. Lett.*, 2005, **1**, 2–4.
14 G. Huber, H. Mantz, R. Spolenak, K. Mecke, K. Jacobs, S. N. Gorb and E. Arzt, *Proc. Natl. Acad. Sci. U. S. A.*, 2005, **102**, 16293–16296.
15 P. H. Niewiarowski, S. Lopez, L. Ge, E. Hagan and A. Dhinojwala, *PLoS One*, 2008, **3**, e2192.
16 A. Y. Stark, T. W. Sullivan and P. H. Niewiarowski, *J. Exp. Biol.*, 2012, **215**, 3080–3086.
17 A. K. Geim, S. V. Dubonos, I. V. Grigorieva, K. S. Novoselov, A. A. Zhukov and S. Y. Shapoval, *Nat. Mater.*, 2003, **2**, 461–463.
18 H. E. Jeong and K. Y. Suh, *Nano Today*, 2009, **4**, 335–346.
19 L. F. Boesel, C. Greiner, E. Arzt and A. del Campo, *Adv. Mater.*, 2010, **22**, 2125–2137.
20 M. K. Kwak, C. Pang, H. E. Jeong, H. N. Kim, H. Yoon, H. S. Jung and K. Y. Suh, *Adv. Funct. Mater.*, 2011, **21**, 3606–3616.
21 S. H. Hu and Z. H. Xia, *Small*, 2012, **8**, 2464–2468.
22 A. del Campo, C. Greiner, I. Alvarez and E. Arzt, *Adv. Mater.*, 2007, **19**, 1973–1977.
23 S. Gorb, M. Varenberg, A. Peressadko and J. Tuma, *J. R. Soc., Interface*, 2007, **4**, 271–275.
24 M. P. Murphy, B. Aksak and M. Sitti, *Small*, 2009, **5**, 170–175.
25 H. E. Jeong, J. K. Lee, H. N. Kim, S. H. Moon and K. Y. Suh, *Proc. Natl. Acad. Sci. U. S. A.*, 2009, **106**, 5639–5644.
26 M. P. Murphy, S. Kim and M. Sitti, *ACS Appl. Mater. Interfaces*, 2009, **1**, 849–855.
27 M. Xu, D. N. Futaba, T. Yamada, M. Yumura and K. Hata, *Science*, 2010, **3**, 1364–1368.
28 L. T. Qu, L. M. Dai, M. Stone, Z. H. Xia and Z. L. Wang, *Science*, 2008, **322**, 238–242.
29 L. T. Qu and L. M. Dai, *Adv. Mater.*, 2007, **19**, 3844–3849.
30 Y. Maeno and Y. Nakayama, *Appl. Phys. Lett.*, 2009, **94**, 012103.
31 M. Xu, D. N. Futaba, M. Yumura and K. Hata, *ACS Nano*, 2012, **6**, 5837–5844.
32 B. Bhushan, B. Galasso, C. Bignardi, C. V. Nguyen, L. Dai and L. Qu, *Nanotechnology*, 2008, **19**, 125702.
33 W. Lu, L. Qu, K. Henry and L. Dai, *J. Power Sources*, 2009, **189**, 1270–1277.
34 L. Qu, F. Du and L. Dai, *Nano Lett.*, 2008, **8**, 2682–2687.
35 K. Gong, S. Chakrabarti and L. Dai, *Angew. Chem., Int. Ed.*, 2008, **47**, 5446–5450.
36 S. Sihn, S. Ganguli, A. K. Roy, L. Qu and L. Dai, *Compos. Sci. Technol.*, 2008, **68**, 658–665.
37 L. Ge, L. Ci, A. Goyal, R. Shi, L. Mahadevan, P. M. Ajayan and A. Dhinojwala, *Nano Lett.*, 2010, **10**, 4509–4513.
38 A. Y. Cao, P. L. Dickrell, W. G. Sawyer, M. N. Ghasemi-Nejhad and P. M. Ajayan, *Science*, 2005, **310**, 1307–1310.
39 T. Tong, Y. Zhao, L. Delzeit, A. Kashani, M. Meyyappan and A. Majumdar, *Nano Lett.*, 2008, **8**, 511–515.
40 K. Autumn, C. Majidi, R. E. Groff, A. Dittmore and R. Fearing, *J. Exp. Biol.*, 2006, **209**, 3558–3568.
41 H. Kinoshita, I. Kume, M. Tagawa and N. Ohmae, *Appl. Phys. Lett.*, 2004, **85**, 2780–2781.
42 H. Lu, J. Goldman, F. Ding, Y. Sun, M. X. Pulikkathara, V. N. Khabashesku, B. I. Yakobson and J. Lou, *Carbon*, 2008, **46**, 1294–1301.
43 P. L. Dickrell, S. B. Sinnott, D. W. Hahn, N. R. Raravikar, L. S. Schadler, P. M. Ajayan and W. G. Sawyer, *Tribol. Lett.*, 2005, **18**, 59–62.
44 Y. Maeno, A. Ishikawa and Y. Nakayama, *Appl. Phys. Express*, 2010, **3**, 065102.
45 B. Bhushan, X. Ling, A. Jungen and C. Hierold, *Phys. Rev. B: Condens. Matter Mater. Phys.*, 2008, **77**, 165428.
46 H. Ko, J. Lee, B. E. Schubert, Y. L. Chueh, P. W. Leu, R. S. Fearing and A. Javey, *Nano Lett.*, 2009, **9**, 2054–2058.
47 M. C. Strus, L. Zalamea, A. Raman, R. B. Pipes, C. V. Nguyen and E. A. Stach, *Nano Lett.*, 2008, **8**, 544–550.
48 M. Ishikawa, R. Harada, N. Sasaki and K. Miura, *Phys. Rev. B: Condens. Matter Mater. Phys.*, 2009, **80**, 193406.
49 M. Ishikawa, R. Harada, N. Sasaki and K. Miura, *Appl. Phys. Lett.*, 2008, **93**, 083122.
50 M. C. Strus, C. I. Cano, R. B. Pipes, C. V. Nguyen and A. Raman, *Compos. Sci. Technol.*, 2009, **69**, 1580–1586.
51 B. Yurdumakan, N. R. Raravikar, P. M. Ajayan and A. Dhinojwala, *Chem. Commun.*, 2005, 3799–3801.
52 Y. Zhao, T. Tong, L. Delzeit, A. Kashani, M. Meyyappan and A. Majumdar, *J. Vac. Sci. Technol., B: Microelectron. Nanometer Struct.–Process., Meas., Phenom.*, 2006, **24**, 331–335.
53 C. T. Wirth, S. Hofmann and J. Robertson, *Diamond Relat. Mater.*, 2008, **17**, 1518–1524.
54 B. Aksak, M. Sitti, A. Cassell, J. Li, M. Meyyappan and P. Callen, *Appl. Phys. Lett.*, 2007, **91**, 061906.
55 L. Ge, S. Sethi, L. Ci, P. M. Ajayan and A. Dhinojwala, *Proc. Natl. Acad. Sci. U. S. A.*, 2007, **104**, 10792–10795.
56 H. Gao and H. Yao, *Proc. Natl. Acad. Sci. U. S. A.*, 2004, **101**, 7851–7856.
57 H. Gao, X. Wang, H. Yao, S. Gorb and E. Arzt, *Mech. Mater.*, 2005, **37**, 275–285.
58 W. R. Hansen and K. Autumn, *Proc. Natl. Acad. Sci. U. S. A.*, 2005, **102**, 385–389.
59 S. H. Hu, S. Lopez, P. H. Niewiarowski and Z. H. Xia, *J. R. Soc., Interface*, 2012, **9**, 2781–2790.
60 J. Lee and R. S. Fearing, *Langmuir*, 2008, **24**, 10587–10591.
61 S. Sethi, L. Ge, L. Ci, P. M. Ajayan and A. Dhinojwala, *Nano Lett.*, 2008, **8**, 822–825.
62 M. Nosonovsky and B. Bhushan, *Nano Lett.*, 2007, **7**, 2633–2637.

63 T. Koishi, K. Yasuoka, S. Fujikawa, T. Ebisuzaki and X. C. Zeng, *Proc. Natl. Acad. Sci. U. S. A.*, 2009, **106**, 8435–8440.
64 W. Barthlott and C. Neinhuis, *Planta*, 1997, **202**, 1–8.
65 P. Y. Hsu, L. Ge, X. Li, A. Y. Stark, C. Wesdemiotis, P. H. Niewiarowski and A. Dhinojwala, *J. R. Soc., Interface*, 2012, **9**, 657–664.
66 B. Chen, P. Wu and H. Gao, *J. R. Soc., Interface*, 2009, **6**, 529–537.
67 J. Liu, C. Y. Hui, L. Shen and A. Jagota, *J. R. Soc., Interface*, 2008, **5**, 1087–1097.
68 B. Zhao, N. Pesika, H. Zeng, Z. Wei, Y. Chen, K. Autumn, K. Turner and J. Israelachvili, *J. Phys. Chem. B*, 2009, **113**, 3615–3621.
69 R. Spolenak, S. Gorb and E. Arzt, *Acta Biomater.*, 2005, **1**, 5–13.
70 C. S. Majidi, R. E. Groff and R. S. Fearing, *J. Appl. Phys.*, 2005, **98**, 103521.
71 M. Lucas, X. Zhang, I. Palaci, C. Klinke, E. Tosatti and E. Riedo, *Nat. Mater.*, 2009, **8**, 876–881.
72 Y. M. Fu and P. Zhang, *J. Adhes. Sci. Technol.*, 2011, **25**, 1061–1072.
73 P. H. Huang, *Compos. Sci. Technol.*, 2012, **72**, 599–607.
74 S. H. Hu, H. D. Jiang, Z. H. Xia and X. S. Gao, *ACS Appl. Mater. Interfaces*, 2010, **2**, 2570–2578.
75 S. H. Hu, Z. H. Xia and X. S. Gao, *ACS Appl. Mater. Interfaces*, 2012, **4**, 1972–1980.

